1 Appendix

1.1 Material

The measured poured bulk density of the powder is 564 kg/m³. After grinding the material to a fine powder, the helium pycnometer AccuPyc 1330 (Micromeritics Instrument Corporation, United States) is employed to measure its skeletal density of 1480 kg/m³. The moisture level of the powder remains continuously at around 3 wt% during storage.

In the fluidized bed liquid water is fed through the top spray into the process chamber. The liquid is atomized by the pressure of the air in the two-fluid nozzle. The glass transition temperature of the maltodextrin was measured at different moisture contents using a differential scanning calorimeter DSC 204F1 Phoenix (NETZSCH-Gerätebau GmbH, Germany). The discrete data points are fit using the Gordon and Taylor equation (Gordon & Taylor, 1952) shown in Equation (1). The equation describes the glass transition temperature as a function of the glass transition temperature of the pure components $T_{g,w}$ and $T_{g,s}$, the mass fraction of liquid x_{wb} and a fitting constant k:

$$T_g = \frac{k x_{wb} T_{g,w} + (1 - x_{wb}) T_{g,s}}{k x_{wb} + (1 - x_{wb})} \quad (1)$$

The glass transition temperature of the solid material $T_{g,s}$ equals 167 °C and of water $T_{g,w}$ is -135 °C. The resulting curve is displayed in Figure 1.

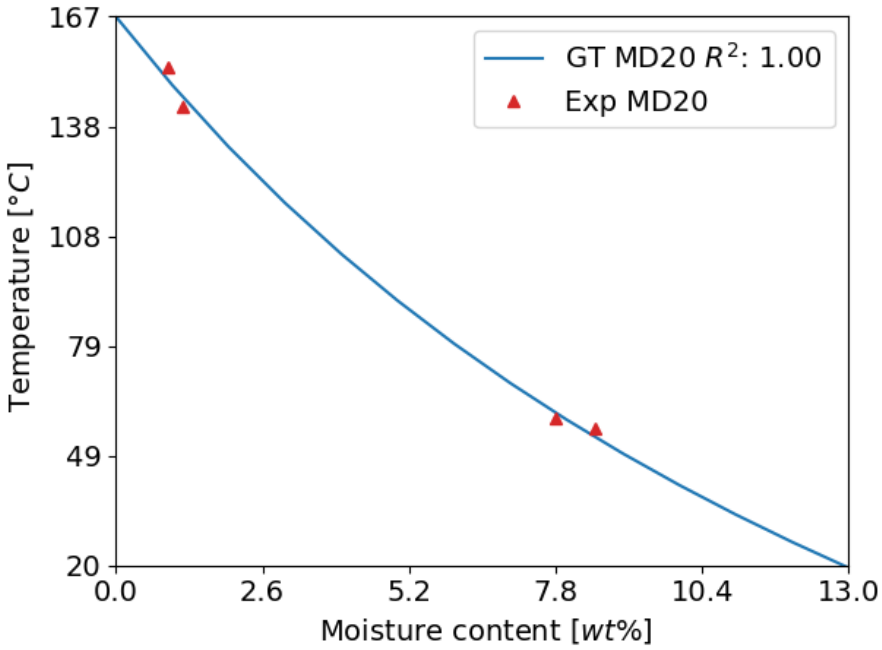

Figure 1: Glass transition temperature of MD20 over increasing moisture content. GT refers to the Gordon and Taylor equation (Gordon & Taylor, 1952). The equation fits with an R^2 of 1.00 using parameter k of 6.4.

The material is conditioned using a climate chamber for the CFB calibration. The correlation between temperature relative humidity and granule moisture content in equilibrium at 20°C can be described with the sorption isotherm in Figure 2.

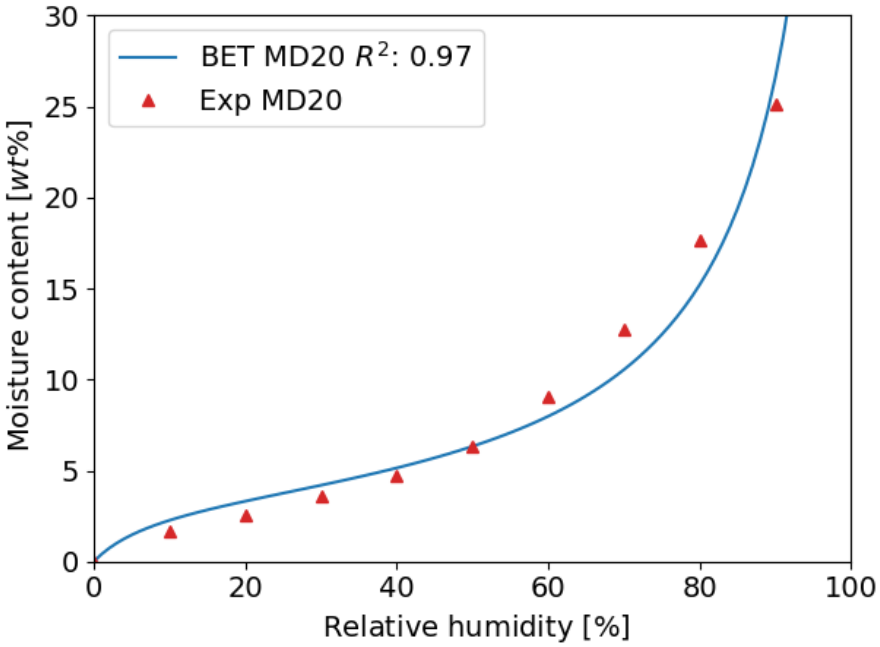

Figure 2: Adsorption isotherm of MD20 at 20°C. BET refers to the Brunauer–Emmett–Teller equation (Brunauer et al., 1938). *The model fits with an R^2 of 0.97 using parameters m_m and n with values of 3.7 and 11.9 respectively at 20°C.*

The sorption isotherm was measured using a dual vapor gravimetric sorption analyzer DVS Resolution (Surface Measurements Systems Ltd., United Kingdom). The Brunauer–Emmett–Teller model (Brunauer et al., 1938), shown in Equation (2), is fit to experimental measurements. X_{db} is the water loading, m_m refers to the monolayer value, which is the quantity of water molecules present in a single layer on the surface, α_w refers to the water activity and n is a fitting parameter:

$$X_{db} = m_m \frac{n\alpha_w}{(1-\alpha_w)(1+(n-1)\alpha_w)} \quad (2)$$

1.2 Lab scale fluidized bed

It is assumed that the particle bed is well mixed and their moisture is homogenously distributed. This is confirmed by comparing the moisture content of the last sample with samples from the entire particle bed. The temperature sensor is positioned at a similar bed height as the microwave sensor at about 5 cm. The temperature in the particle bed is homogeneously distributed. Deviations of less than 1 °C are measured when comparing the temperature sensor of the fluidized bed at a height of 12 cm with a second temperature sensor of the moisture probe at a height and depth of 5 cm (data not shown). These small temperature differences confirm the assumption of a homogeneously distributed bed.

1.3 Microwave sensor

In order to examine the measurements dependence on the particle position two experimental setups are used as shown in Figure 3 and Figure 4: the (i) first setup allows to examine the effect of the distance perpendicular to the sensor and the (ii) second setup allows to investigate the effect of the distance from the sensor center parallel to the sensor tip while maintaining contact with the particles.

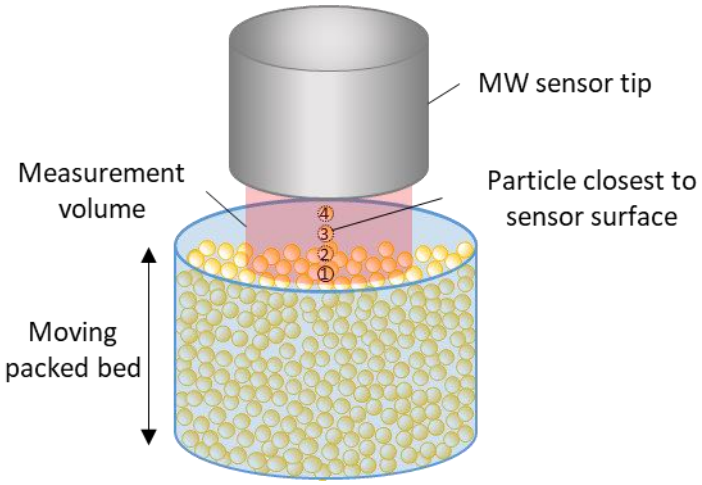

Figure 3: Experimental setup to investigate impact of particle position and MW measurement volume filling level by approaching the sensor with a packed bed perpendicular to the sensor surface.

The investigated particle positions inside the measurement volume are numbered from 1 to 7.

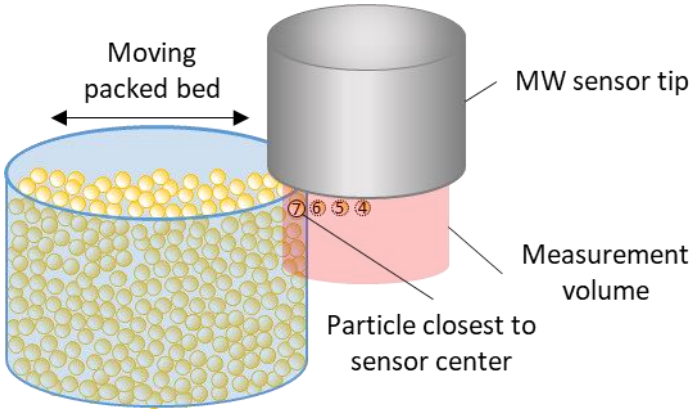

Figure 4: Experimental setup to investigate impact of particle position by approaching the sensor with a packed bed perpendicular to the sensor axis, while maintaining contact with the sensor surface.

The maximum penetration depth of the sensor is about 1.5 cm into the bed normal to the sensor tip. This is determined by approaching the sensor tip normal to the sensor tip until a signal is retrieved as shown in Figure 3. In Figure 5 the impact of the distance perpendicular to the sensor tip is displayed for the initial and agglomerated powder at 2.3 and 5.6 GHz. The moisture signal is clearly influenced by the distance between the solid and the sensor tip in all four cases. In case of the initial powder at 2.3 GHz the measurement is independent of the measurement volume if the sensor plane to particle distance is below a certain threshold at 2.3 GHz. The signal fluctuations of the initial and the agglomerated powder increase with increasing distance. At 5.6 GHz there is a clear increase of the signal with increasing distance for both powders. This means that the measurement volume does not have to be filled completely, but material needs to be rather close to the sensor tip to achieve reproducible and distance independent measurements at 2.3 GHz while at 5.6 GHz the signal converges to the signal at direct contact with the sensor.

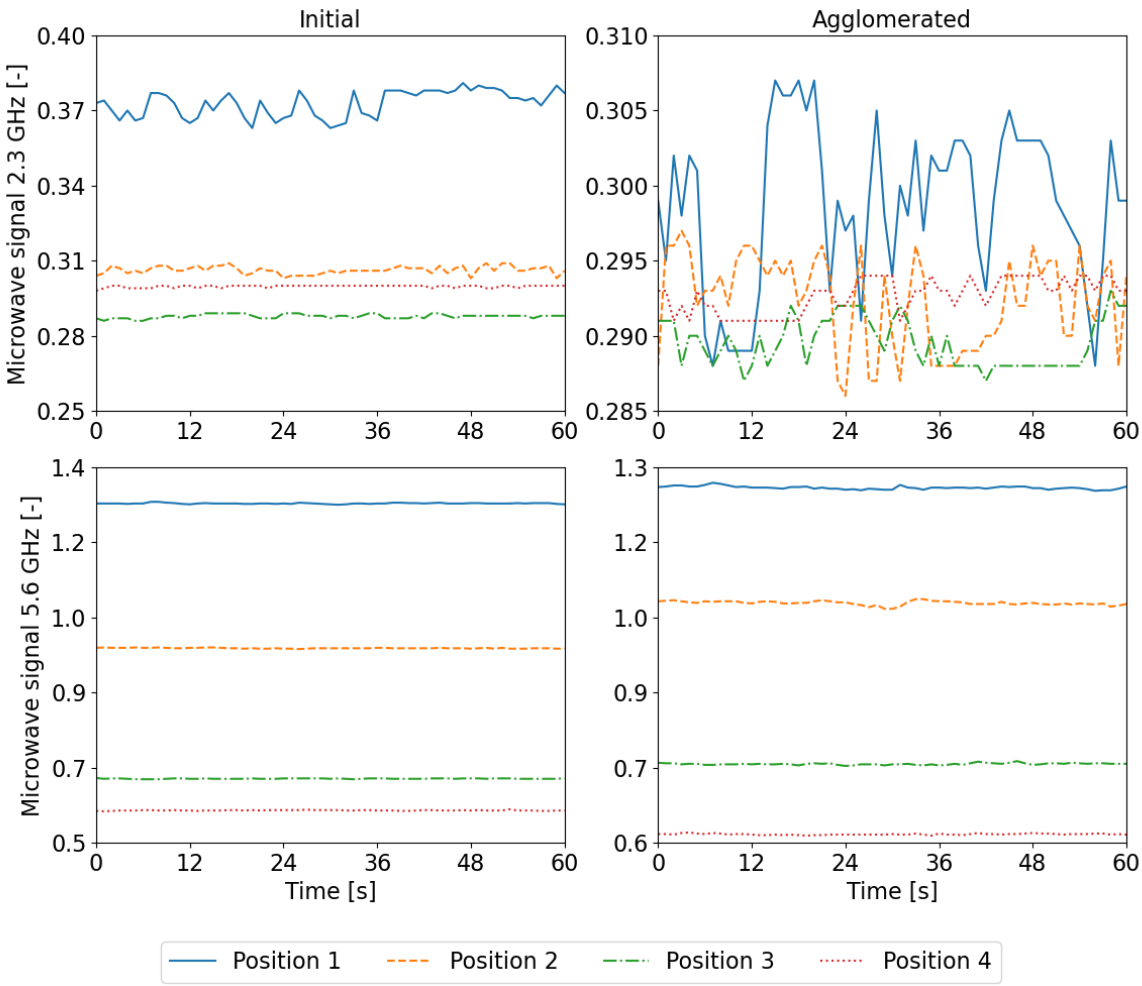

Figure 5: Microwave signal evolution over one minute at 2.3 and 5.6 GHz for initial (left) and agglomerated (right) material. The positions correspond to Figure 3 where position 4 is in contact with the sensor and 1 is the farthest away.

The measurement is independent of the particle position parallel to the sensor plane in case of agglomerated powder at all frequencies. This is examined by approaching the measurement volume from the side of the probe as shown in Figure 4. The results are shown in Figure 6.

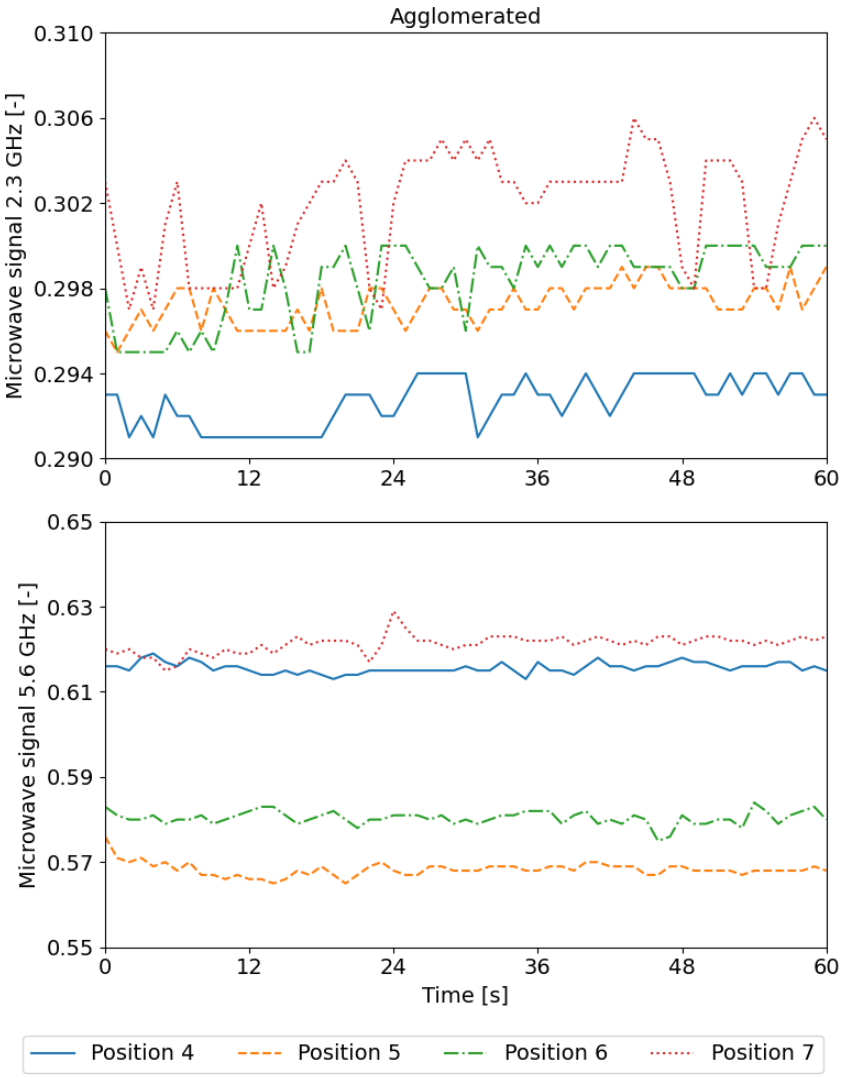

Figure 6: Microwave signal evolution over one minute at 2.3 and 5.6 GHz for agglomerated material. The positions correspond to Figure 4 where position 4 is the sensor center and 7 is the farthest away from the center.

The device can determine the moisture content independent of the mass, which is a function of bulk density due to a constant measurement volume. Two samples are conditioned, one with fine initial powder and a second coarse agglomerated powder produced in the fluidized bed with bulk densities of 550 kg/m³ and 270 kg/m³ respectively. The two samples have a moisture content of 10.08 wt% and 9.88 wt% for fine and agglomerated material respectively. The measured MW moisture signals at 2.3 GHz are 0.297 and 0.288 with a standard deviation of 0.05% and 0.23% respectively. The measured MW moisture signal at 5.6 GHz are 0.532 and 0.528 with a standard deviation of 0.11% and 0.14% respectively. This shows that the MW sensor can measure the moisture content independent of the bulk density at both frequencies.

The device corrects for the change in resonance frequency caused by sensor hull expansion due to different temperatures. The reference resonance frequency in an empty state is set before every experiment. Prior to the adjustment the sensor is preheated as close as possible to the process temperature. The inlet temperature was chosen to approximate the temperature in the process chamber since the process temperature depends on multiple factors such as inlet temperature, inlet air flow rate, bed mass, initial particle moisture content, liquid spray flow rate and others.

1.4 Gravimetric method

A precision balance is used to determine the granule moisture content of the samples of about 1 g offline. The samples are weighted before and after drying. The moisture content can then be determined using Equation (3). The samples are dried in the oven for 5 days at 110 °C. The samples are spread in the container to create a thin layer to accelerate drying. The method is compared to an established moisture analyzer. The measurements coincide with moisture analyzer EM 120-HR (Precisa Gravimetrics AG, Germany):

$$x_{wb} = \frac{m_{wet} - m_{dry}}{m_{wet}} * 100 \quad (3)$$

1.5 Design of experiment

The process parameters of all experiments are listed in Table 1.

Table 1: Process parameters of fluidized bed experiments.

Experiment	Air flow rate [m³/h]	Temperature [°C]	Water flow rate [g/min]
1	80	70	12
2	80	70	12
3	60	40	6
4	100	100	6
5	60	100	18
6	100	40	6
7	60	100	6
8	100	40	18
9	100	100	18
10	75	60	10
11	75	80	10
12	75	80	14
13	85	60	10
14	85	80	10
15	85	80	14
16	80	70	12
17	60	40	6
18	100	100	6
19	100	40	6
20	60	100	6
21	100	100	18
22	75	60	10
23	75	60	14
24	75	80	10
25	75	80	14
26	85	60	10
27	85	60	14
28	85	80	10
29	85	80	14

1.6 Calibration

The contour plot of the microwave moisture signal at 5.6 GHz is shown in Figure 7.

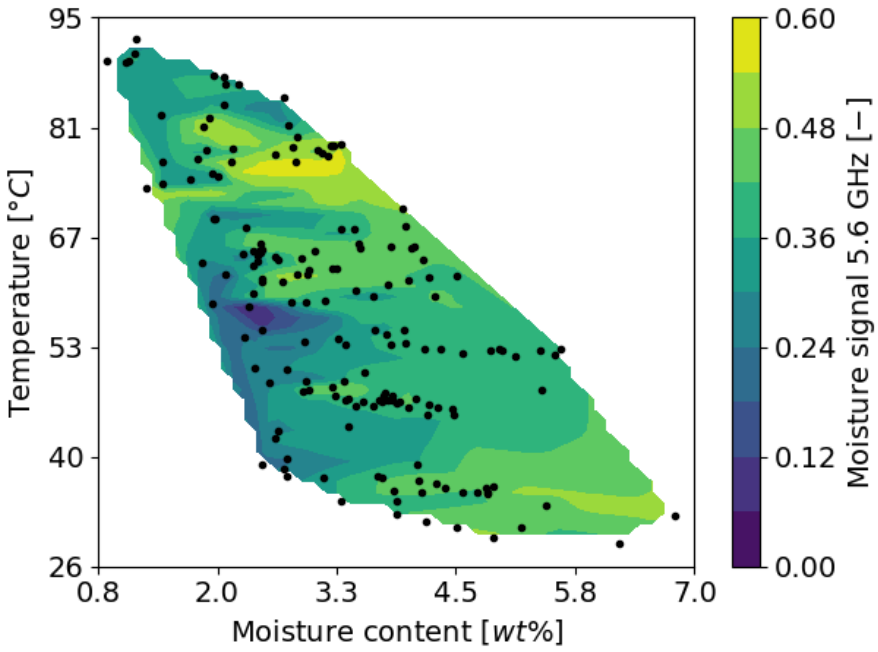

Figure 7: Interpolated contour of the MW moisture signal at 5.6 GHz of MD20 for a moisture content and temperature range. The black dots show the moisture content and temperature of the IFB samples.

The contour plot of the microwave density signal at 2.3 GHz is shown in Figure 8.

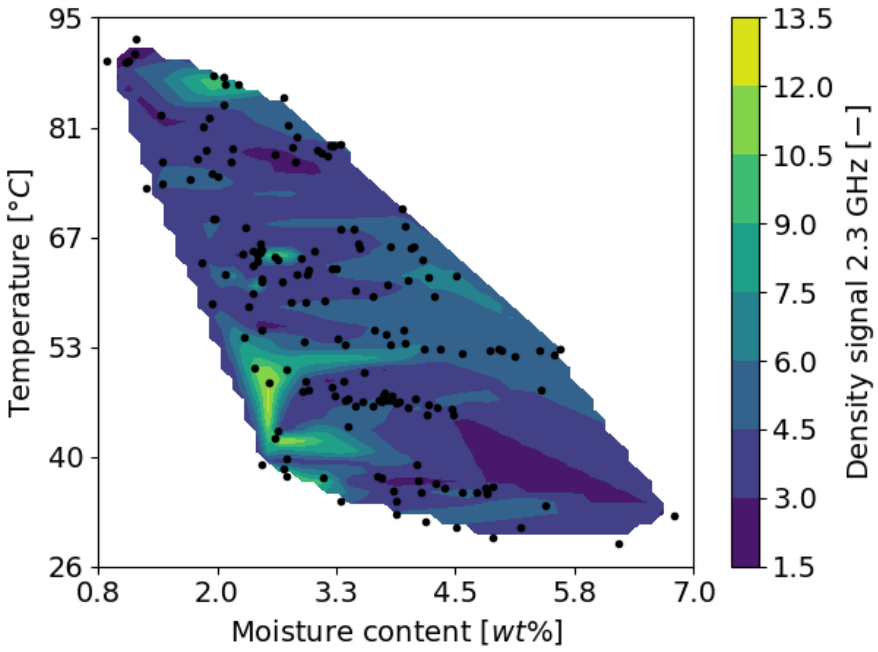

Figure 8: Interpolated contour of the MW density signal at 2.3 GHz of MD20 for a moisture content and temperature range. The black dots show the moisture content and temperature of the IFB samples.

The contour plot of the microwave density signal at 5.6 GHz is shown in Figure 9.

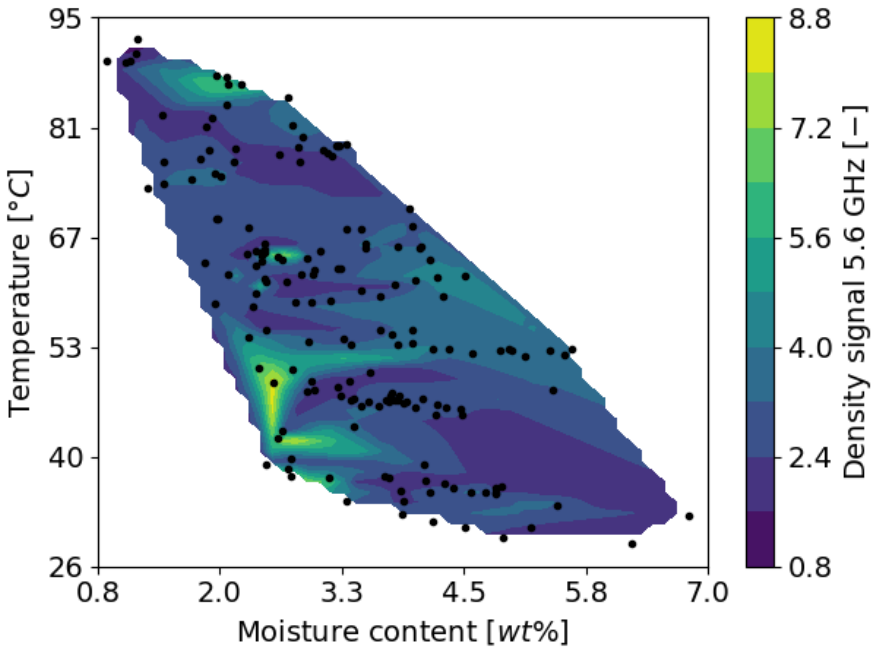

Figure 9: Interpolated contour of the MW density signal at 5.6 GHz of MD20 for a moisture content and temperature range. The black dots show the moisture content and temperature of the IFB samples.

The parity plot of the CFB calibration applied to the IFB dataset is shown in Figure 10.

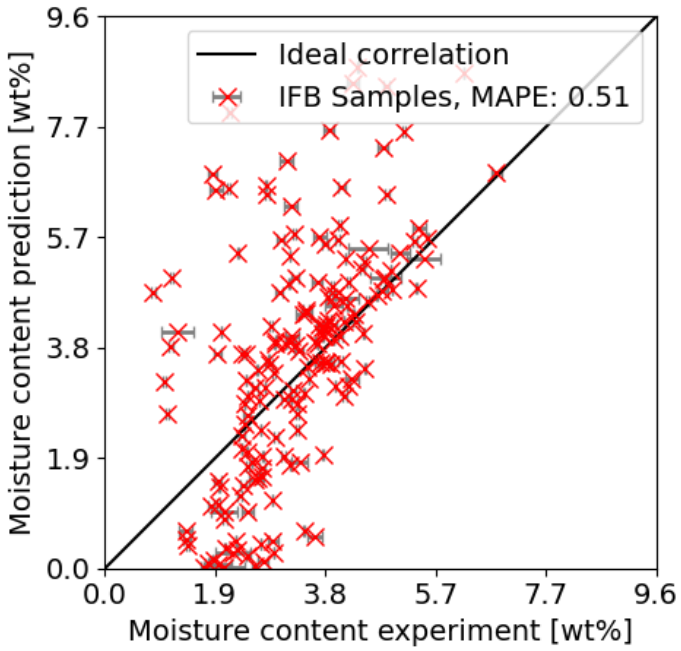

Figure 10: Parity plot showing the predicted moisture content using CFB calibration over the IFB samples. The MAPE is 49%.

The parity plot of the IFB calibration applied to the CFB dataset is shown in Figure 11.

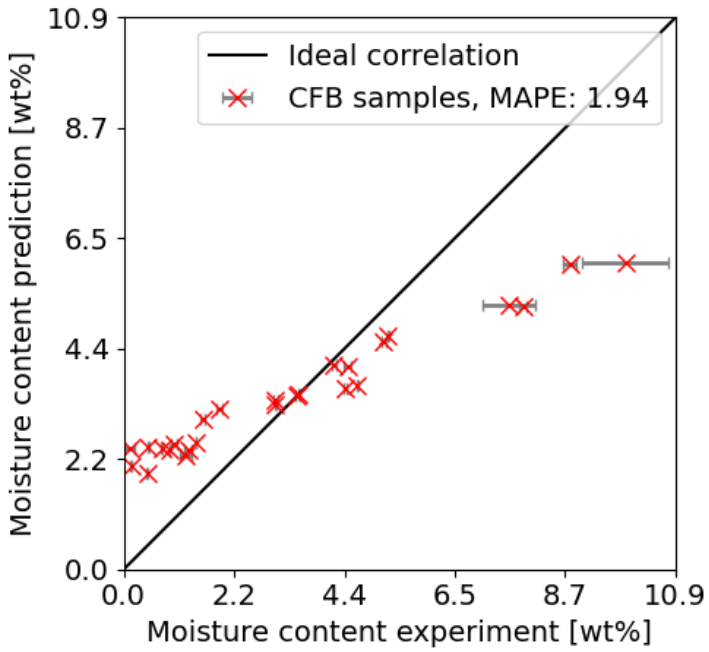

Figure 11: Parity plot showing the predicted moisture content using IFB calibration over the CFB samples.

1.7 Feature selection

The heat map of the Spearman coefficients of the different input parameters for feature selection is shown Figure 12.

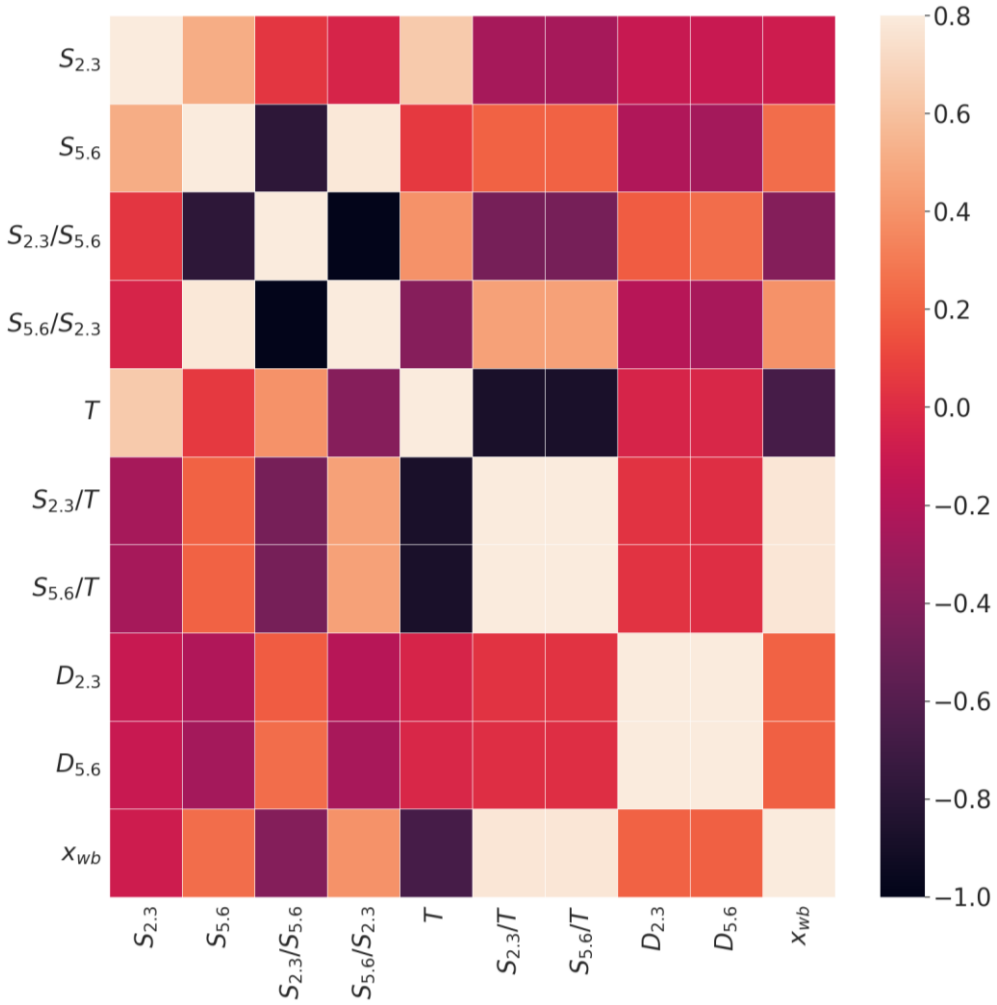

Figure 12: The Spearman coefficient as a heat map.

The histograms of input parameters for feature selection are shown in Figure 13.

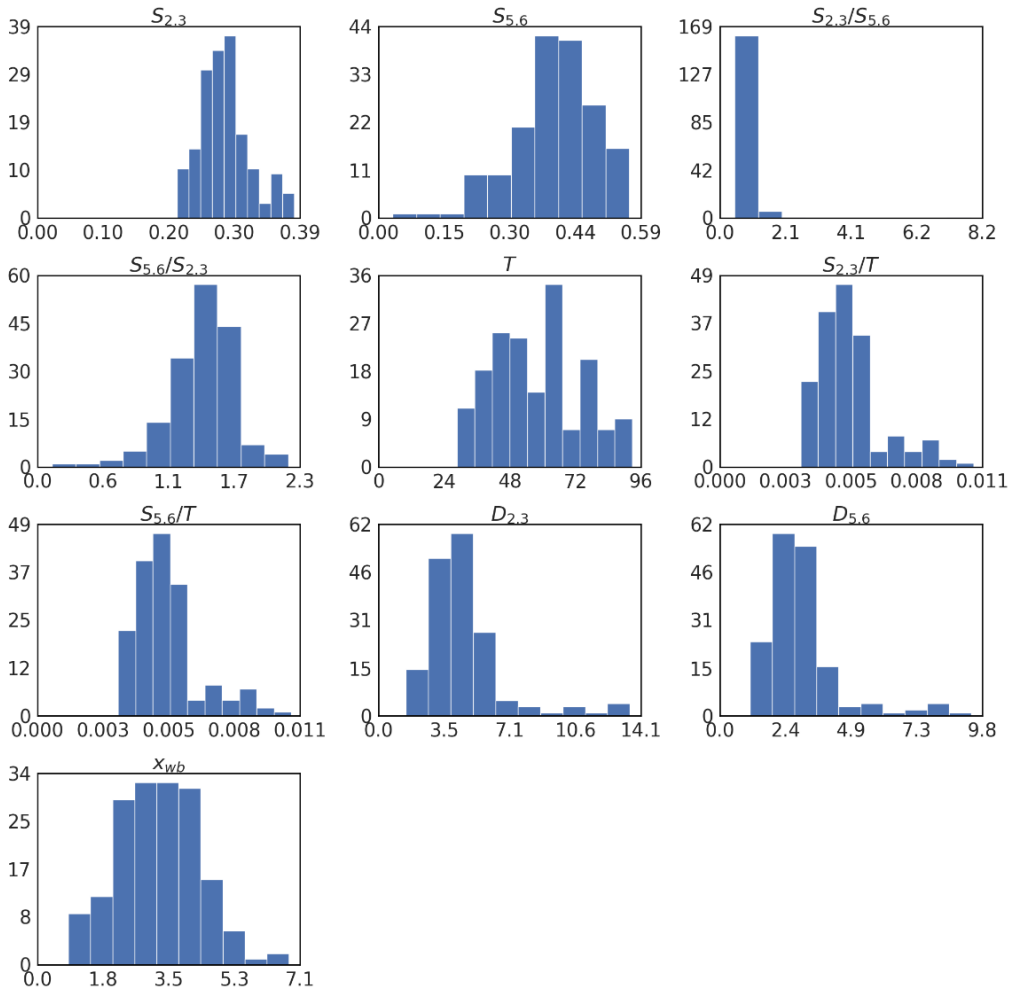

Figure 13: The input parameters displayed as histogram.

The input parameters and the corresponding Pearson and Spearman coefficient for feature selection are shown in Table 2.

Table 2: Pearson and Spearman coefficients of the input parameters to the target values of the IFB data.

Input parameter	Pearson coefficient	Spearman coefficient
$S_{2.3}$	-0.17	-0.09
$S_{5.6}$	0.28	0.25
$S_{2.3}/S_{5.6}$	-0.21	-0.40
$S_{5.6}/S_{2.3}$	0.43	0.40
T	-0.68	-0.67
$S_{2.3}/T$	0.73	0.77
$S_{5.6}/T$	0.73	0.77
$D_{2.3}$	0.02	0.21
$D_{5.6}$	0.01	0.20